CORROSION OF INDUSTRIAL FRIT FURNACE REFRACTORIES: A POSTMORTEM STUDY

Selçuk ÖZCAN [1, *], Sedat AKKURT [2]

[1] Department of Chemical and Process Engineering , Bilecik Şeyh Edebali University, Bilecik, Turkey
[2] Department of Mechanical Engineering, İzmir Institute of Technology, Urla, İzmir, Turkey

ABSTRACT

Microstructural and phase analyses of corroded frit furnace refractories forming the side walls and the bottom of an industrial frit furnace is reported in this study. Reflected light optical microscopy, scanning electron microscopy, energy dispersive spectroscopy, and x-ray diffraction tools were used for the analyses. The microstructural analysis in combination with the saturation solubilities information in the phase diagrams was used to predict the corrosion behavior of the refractories. The frit and the refractory types were compared qualitatively for the dissolution potential and corrosion mechanisms. The dissolution of the refractory material was direct (congruent) for both the side wall refractories and bottom pavers. The first push exudation phenomenon was determined to be effective for the increase of porosity and pore dimensions which in turn caused accelerated wear rates when combined with corrosion. The corrosive potential of the transparent frit for corundum, mullite, and glassy phase in the refractories was determined to be excessive. The dissolution of these species in the molten transparent frit was predicted to start at temperatures between 1000-1340ºC while the operating temperature was 1470ºC. The decrease in the extent of corrosion by zirconia inclusion either in the refractories or in the molten glass compositions was qualitatively discussed.

Keywords: Refractory corrosion, Molten glass, Frit, Frit furnace, Frit furnace refractory

1. INTRODUCTION

Frit is a major component of the glossy surface coating of ceramic whiteware products such as porcelain, table ware, sanitary ware, wall tile and floor tile. It is a mixture of amorphous glassy oxides with minor amounts of crystalline phases of the same oxides, and has an extensively diminished potential of dissolution in water. The frit also reduces gas evolution reactions at elevated temperatures (over 1000ºC) [1-6].

In general, frits are produced in continuous open hearth furnaces with a continuous inlet of finely milled and homogenized powder mixture of raw materials, and a continuous outlet of molten glass. A typical furnace consists of an inner refractory brick or block lining which forms a tank for molten glass, a thermal insulation layer of insulation bricks, and a steel support structure, furnished with burners, flue and reaction gas vents, and combustion gas (either LPG or natural gas) and air flow regulators, temperature and molten frit flow rate (by furnace inclination) controllers. Frits can also be produced in batch drum furnaces with a monolithic refractory lining formed by ramming. In this type of furnaces gas consumption per unit of frit produced is higher in comparison to continuous furnaces [3].

A major concern in frit production in continuous furnaces is the wear of refractory lining. Since the composition of the frit is adjusted to wet ceramic tile body surfaces when molten (or softened), wetting of refractory surface by the melt is inherent during frit production, while wetting is an important constituent of the mechanism that accelerates corrosion of the refractory bricks. During operation, the refractory bricks and blocks get thinner due to corrosion and erosion and subsequent spalling by melt flow induced shear and thermal shock of cooling-heating cycles. In some cases wear

---

is observed to be so extensive to pierce holes in the bottom pavers of the refractory tank lining. The lining has to be replaced in part or totally at intervals, adding to the production cost of frits [7-9].

Wear of refractories in contact with metallurgical slag (e.g. in steel making) and molten glasses (in frit production) was studied extensively [10-12]. Wear can be due to chemical corrosion, physical erosion, or in general by the effect of both of these phenomena [13]. Refractory corrosion is a liquid-solid reaction involving the dissolution of refractory by molten slags or glasses [14]. In the general model the initial stage of corrosion starts with wetting of the refractory hot face.

Initiating at the grain faces (phase boundaries) it progresses by the penetrating dissolution of the vitrified bonding matrix through cracks, voids, pores, and even by atomic scale diffusion, resulting in finger-like protrusions into the refractory at the intermediate stage. In the final stage when the molten glass or slag has penetrated deep into the material, the complete disappearance of the bonding matrix of the hot face takes place. At this stage the crystalline grains are being held together only by the increased viscous resistance of the infringing molten glass. Spalling is eminent by the hydrodynamic instabilities induced by shearing forces of the bulk molten glass flow. Therefore, chemical composition and crystalline microstructure of the refractory material and the molten glass are the major factors determining the corrosion potential [15].

Corrosive dissolution reaction rates are controlled by the mass transfer in the molten liquid, which may be dominated by one or more of the molecular diffusion, natural convection, or forced convection mechanisms. Dissolution of refractory oxides into a molten glass can be homogeneous (congruent or direct), that is the refractory oxides constituting the refractory dissolves directly into the melt. Nevertheless, heterogeneous (incongruent or indirect) dissolution is also possible when one or more solid reaction products form at the refractory-melt interface at the service temperature. The dissolution rate decreases by the formation of such a solid product layer. The phase diagrams can be used to predict the possibility of the formation of interfacial solid products, and to compare the corrosion resistance of refractories in given slags and temperatures, as well as revealing the corrosion mechanisms [16].

The recess thickness is the distance measured from the hot face of the lining to the freeze plane beyond which no liquid exists, and therefore, no material can be transferred and the corrosion halts totally. Only very little amount of mass transfer may be possible by solid state atomic diffusion due to the excessively high melting temperature of refractory materials (e.g. ZrO_2, Al_2O_3 or mullite). The nearer the recess plane to the hot face the less volume of refractory is affected by dissolution (corrosion) reactions and a thinner section wears out, increasing its service life. A steeper temperature gradient in the refractory provides this effect. However, a steeper temperature gradient means a higher rate of heat transfer through the lining, increasing gas consumption during frit production. This effect has to be taken into consideration during the design or renovation of the lining of the furnace, for optimizing the energy versus refractory consumption [17].

Many refractories comprise polycrystalline grains made up of crystal dendrites, hexagonal plates and other crystal forms surrounded by a glassy matrix. The amount of the glassy matrix can be as high as 35 vol% even in the fused cast alumina-zirconia-silica (AZS) refractories. During the initial heating of the glass melting furnace, the liquefied glassy phase is driven out of the refractory body through the existing open pores by the internal gas pressure derived from the oxidation of initially present reduced species, cyclic redox of polyvalent impurities (Fe, Ti, Cr), "reboil" of dissolved gases, and by the "vitrostatic pressures" due to phase transformations and thermal expansion incompatibility of various phases. This leads to a more porous inner structure, although as a minor effect, the initially existing open pores may become closed pores by the exuded material. This exudation of the glassy matrix leaves behind a defective and weakened refractory structure with a lost binding phase and formed cracks. The exudation phenomenon eventually will lead to spalling of the refractory, either by

heating-cooling cycles or by the combined effect of corrosion. Exudation continues throughout the service life of refractories despite the leveling off of exudation rate in time [18].

In this study, post-mortem microstructure [19] of the corroded refractor bricks forming the sides lining of the glass melt tank, and the bottom paver blocks (of a particular frit furnace producing frits to be used as the components of the wall and floor tile glazes), together with unused refractory bricks were examined by reflected light optical microscopy, XRD and SEM-EDS methods [20]. The revealed microstructures were analyzed by the use of phase diagrams as a first step in determining the mechanisms effective in the wear (corrosion) by the molten glass. This information may facilitate the proper choice of refractory materials, operating conditions (temperature, frit flow rate, molten glass level in the refractory tank, etc.), more convenient frit composition, and furnace design to extent the service life of the refractory lining, thus lowering the production cost of the frits.

2. EXPERIMENTAL

2.1. Sample Preparation

Refractory brick specimens were collected from the sidewalls and the bottom pavers of the continuous frit furnace (Lodesani F60/2) at a local ceramic manufacturer. The refractory specimens that were selected for microstructural analysis are listed in Table 1. The samples were cut and mounted in polyester resin before being ground and polished with diamond suspensions (down to 1 micrometer). The XRD samples were prepared first by crushing the required sections of the refractories followed by fine milling in an agate mortar (below 100 mesh).

2.2. Microstructural, Elemental and Phase Analyses

The refractory samples were examined by reflected light optical microscope (RL-OM) by ascribing coordinates to the corners of the samples relative to a distinctive feature on the surface. The sample surfaces were scanned systematically, and photographs were taken using plane polarized light. The refractory samples were also examined by the scanning electron microscope (Philips XL-30S FEG). The samples were sputter coated by AuPd alloy for conduction. Qualitative and quantitative elemental identification of spots and small regions on individual structural elements, crystal grains and glassy matrix were carried out by EDS. The x-ray diffraction patterns were obtained by Philips X-Pert Pro x-ray diffractometer at 2θ values between 5-70° with CuKα radiation.

Table 1. Refractory brick specimens selected for characterization

Melt Furnace Section	Material	Sample code
Glass melt container-Sidewall	Mullite bricks, 70-73% Al_2O_3	GS-M
Unused glass melt container-Sidewall	Mullite bricks, 70-73% Al_2O_3	GS-M-Unused
Glass melt container-Mortar	Unknown	G-Mor
Glass melt container-Bottom paver	Electrofused cast AZS blocks, ER 1681 RTD	GB-AZS

3. RESULTS AND DISCUSSION

GS-M Samples:

The examination with unaided eye of the corroded melt tank refractory brick as received (GS-M samples) showed that there were widespread white appearing granules embedded within a porous structure. In the refractory-molten glass boundary these white grains protruded, giving the impression that they had better corrosion resistance than the surrounding structure. Translucent type of grains also embedded and distributed diffusely in the structure. The rest of the refractory consisted of a homogeneous glassy matrix (Figure 1).

Figure 1. Photograph of corroded refractory brick (GS-M)

The XRD patterns of the unaffected inner bulk, and the corrosion interface of the corroded brick are given in Figure 2a, and Figure 2b, respectively. The results showed the existence of corundum, mullite and small quantities of sillimanite in the unaffected bulk portion, while corundum and mullite were the only existing crystal phases in the corrosion interface. The relative intensities of the peaks that belonged to corundum with respect to the mullite were greater for the corrosion interface as compared to the unaffected bulk pattern. This pointed out that the dissolution of mullite phase was more extensive than the corundum phase in the molten glass-refractory interface.

RL-OM and SEM were used for the microstructural examination of the described corroded refractory brick. The RL-OM and SEM images of the protruding grain on the corrosion interface are shown in Figure 3a and 3b. These grains were as large as 2 mm. The EDS analysis given in Figure 4 indicated 52 wt% Al, and 48wt% O, which was in agreement with the theoretical values for pure Al_2O_3 (Al: 52.9 wt%, O: 47.1 wt%). Together with the XRD results these grains were identified as corundum. Most probably, these Al_2O_3 grains had not formed or co-crystallized during the production of the brick, but rather preprepared corundum particles were mixed in the green composition of the refractory before firing.

The widespread translucent grains in the structure were determined to be single crystals by the RL-OM and SEM images as shown in Figure 5a and 5b. The size of the grains could be as large as 2 mm. The point EDS analysis of the grain given in Figure 6 indicated that the elemental composition was 37 wt% Al, 11 wt% Si, and 52 wt% O, close to the theoretical values of mullite, $3Al_2O_3.2SiO_2$ (Al: 38.0 wt%, Si: 13.2 wt%, O: 48.8 wt%). The XRD patterns in Figure 2a and 2b showed mullite as the major crystalline phase for both of the inner bulk and corrosion interface regions, supporting the translucent grains to be mullite crystals. The slight discrepancy from the mullite composition in the EDS analysis might be due to the existence of embedded Al_2O_3 crystals in small quantities. These were the crystals formed during the heat treatment step of the refractory production.
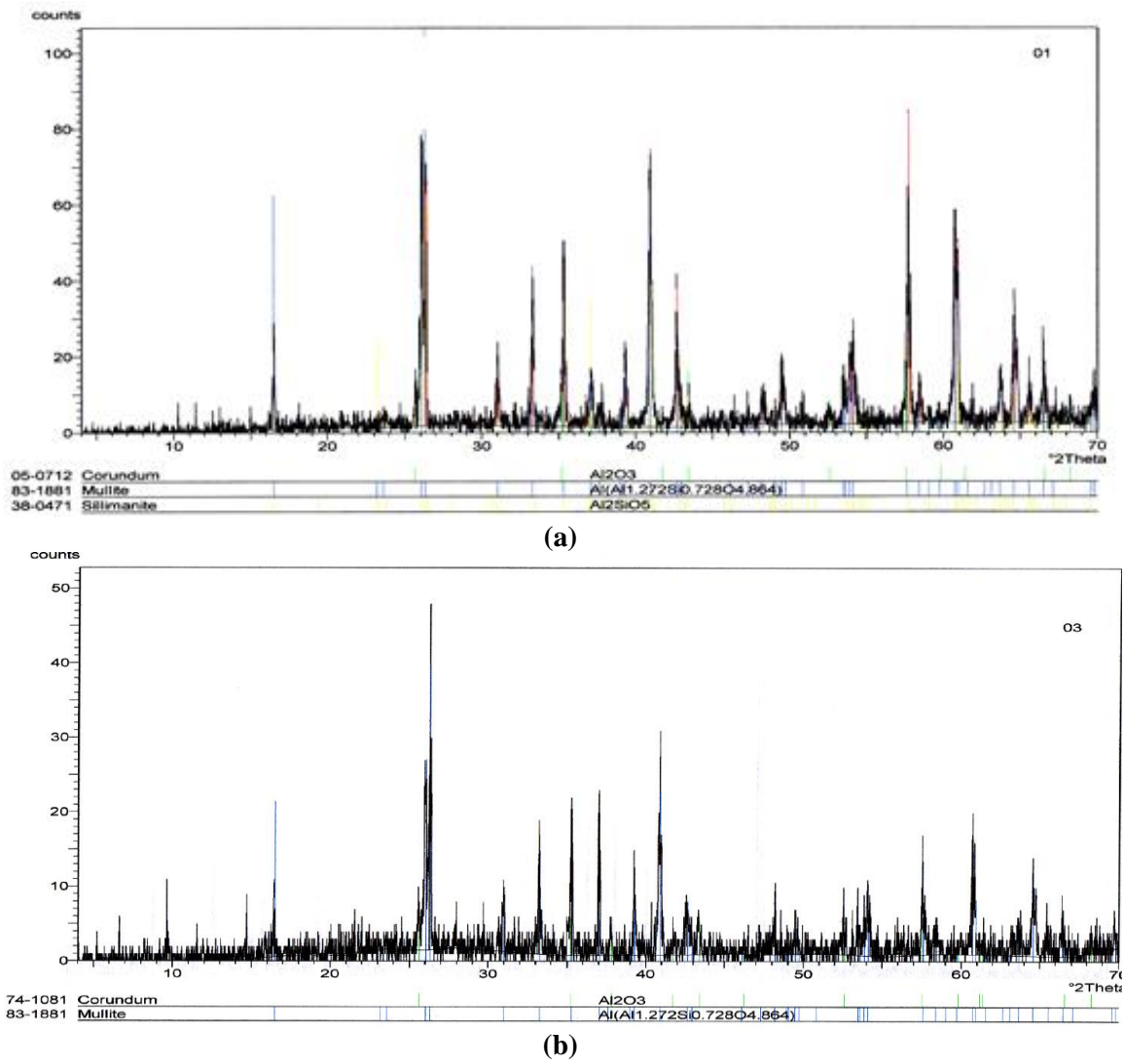
(a)

(b)

Figure 2. (a) The XRD pattern of the corroded refractory brick (GS-M sample), **(a)** the unaffected inner region, **(b)** the molten glass-refractory interface

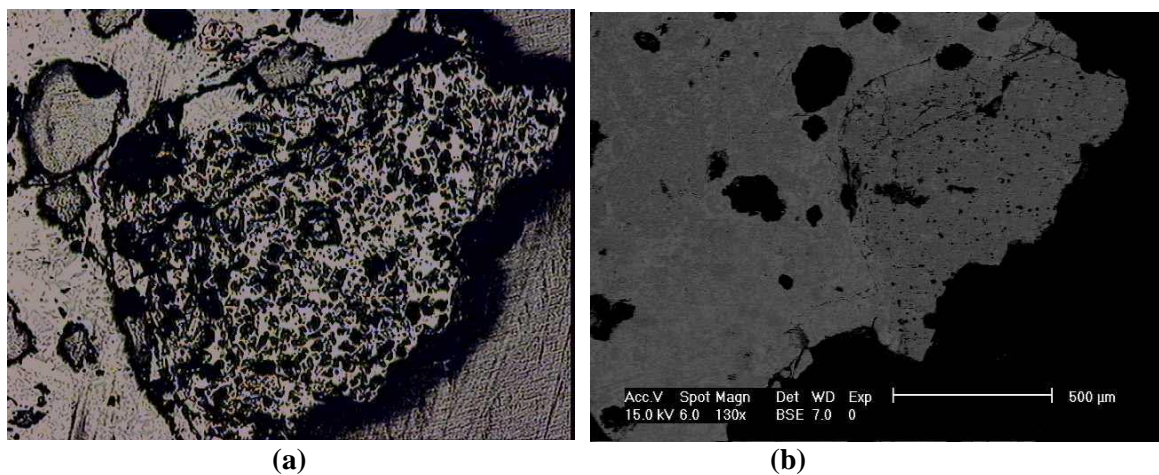**(a)**   **(b)**

Figure 3. (a) RL-OM image of corroded melt tank refractory brick; white color filler grain at the refractory-molten glass interface (magnification 150x), **(b)** SEM image of the same region
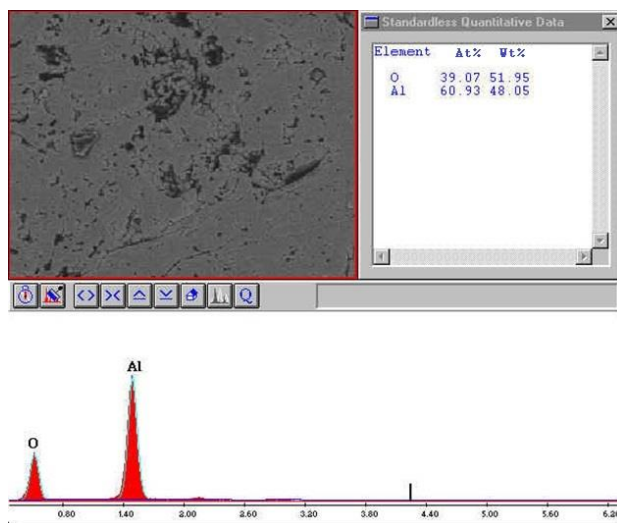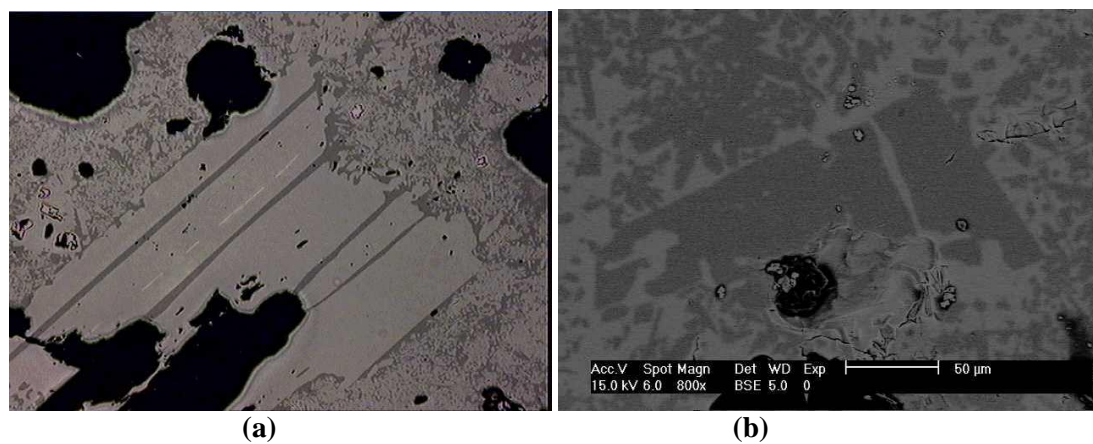
Figure 4. EDS zone analysis of the white color grain

| (a) | (b) |

Figure 5. **(a)** RL optical microscope image of idiomorphic mullite crystals in the unaffected bulk of the corroded refractory (150x) **(b)** SEM image of idiomorphic mullite crystals in the bulk
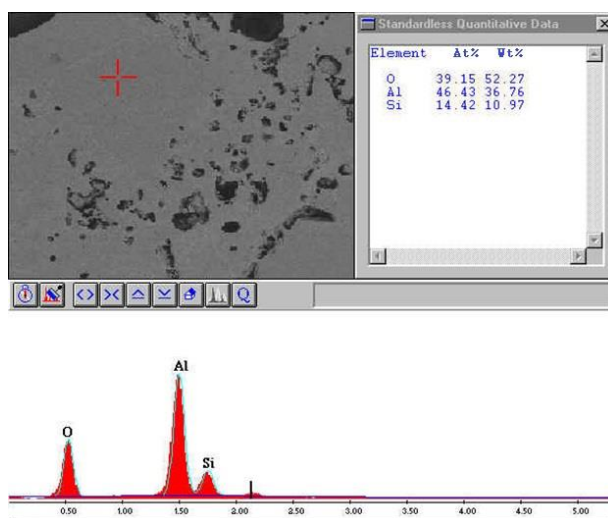

Figure 6. EDS point analysis of the idiomorphic grain

RL-OM and SEM images of the matrix surrounding the filler corundum and mullite grains are shown in Figure 7a and 7b. The elemental composition of the matrix was determined by EDS analysis as shown in Figure 8a and 8b. The structure that could be described as the dark gray portion of the matrix in the SEM images turned out to be mullite crystals with small amounts of glass phase (Figure 8a). The light gray portion of the matrix was found to be a glassy phase of majorly Si and Ca, with smaller amounts of Mg, K, and Na (Figure 8b). In RL-OM images of the mullite crystals there were light grey colored grains surrounded by the darker colored glassy matrix. The mullite crystal sizes on the average were ~7 μm. The glassy portion constituted about 35 vol% of the matrix as determined by SEM image analysis. The refractory structure was porous with pore sizes up to 1 mm.

The microstructure of the corroded refractory brick (GS-M) showed no change from the refractory-molten glass interface towards the inner bulk region. There was not a detectable freeze plane inside the refractory. This observation pointed out that the corrosion mechanism was direct dissolution of the refractory material.
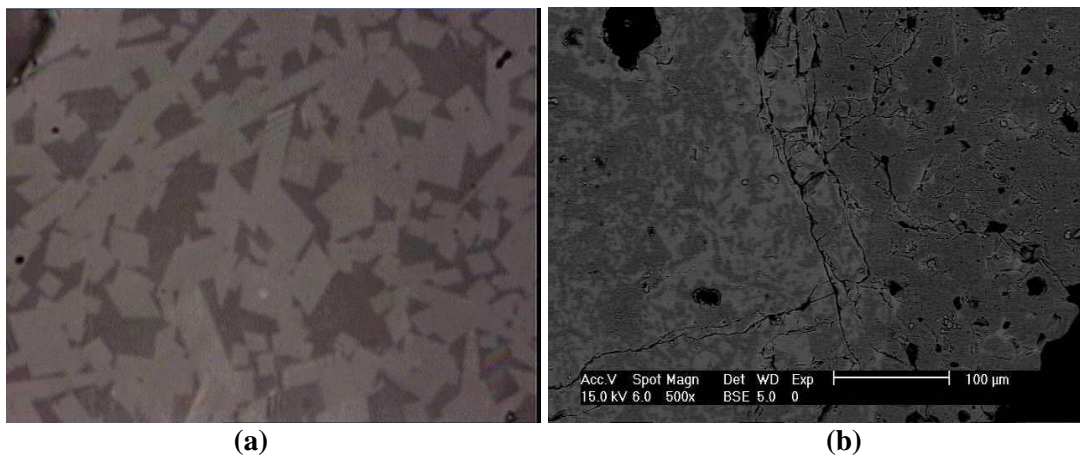

(a)   **(b)**

Figure 7. (a) RL optical microscope image of glassy matrix incorporating mullite crystals in the unaffected bulk of the refractory (3000x) **(b)** SEM image of the glassy matrix incorporating mullite crystals in the unaffected bulk of the refractory
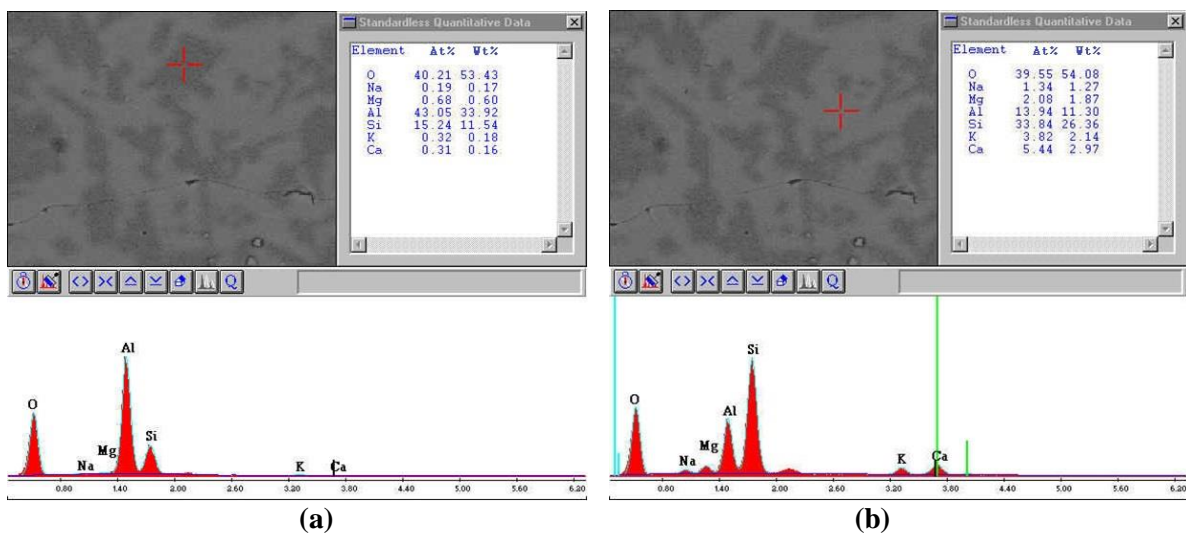

(a)   **(b)**

Figure 8. (a) The EDS point analysis of the dark gray portion of the matrix, **(b)** The EDS point analysis of the light gray portion of the matrix

GS-M-Unused Samples:

The XRD diffraction pattern of the unused refractory brick of the same type of the analyzed corroded brick is given in Figure 9. The major crystal phase was mullite with minor amounts of corundum and trace amounts of sillimanite and cordierite. The increased ratio of mullite to alumina in comparison to the corroded brick provided evidence of the higher dissolution rate of mullite with respect to alumina.

The RL-OM and SEM images of the unused brick are shown in Figure 10a and 10b. The EDS analyses results are given in Figure 11. The crystals of approximately 7 μm size embedded in the matrix were determined to be alumina (Figure 11a). The surrounding matrix was found to be of glass structure incorporating mullite crystals (Figure 11b) deduced by stoichiometric considerations. The EDS analysis of the grain inside the structure revealed that it comprised a mixture of corundum, mullite and glass. The small quantity of polyvalent elements Fe and Ti might cause first push exudation during the initial heating of the furnace leaving behind a porous structure as was the case of corroded brick. The lower porosity of the unused brick as compared to the corroded brick supported the exudation mechanism.
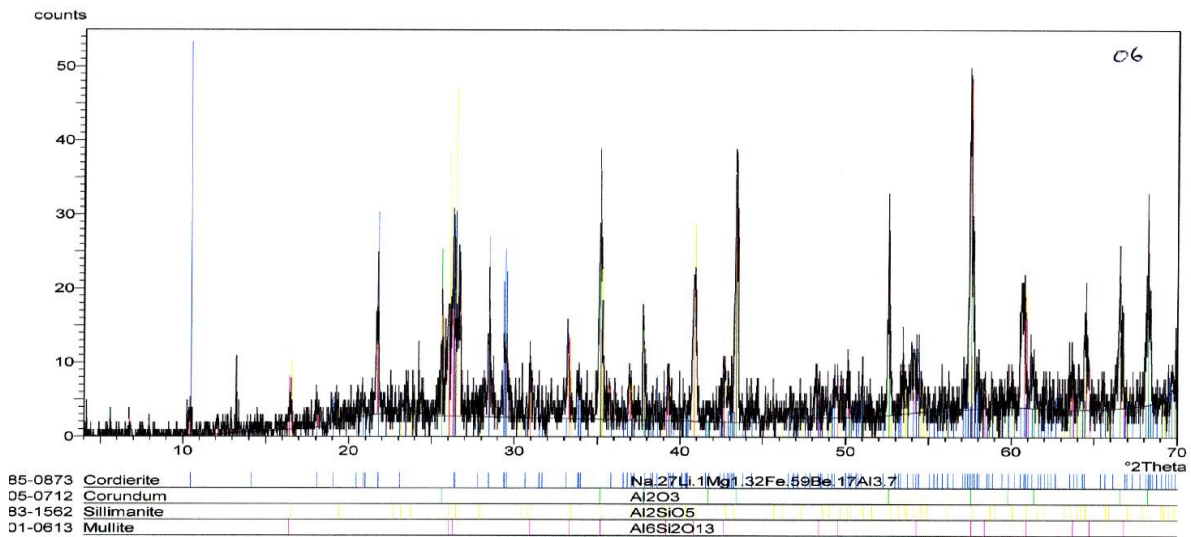

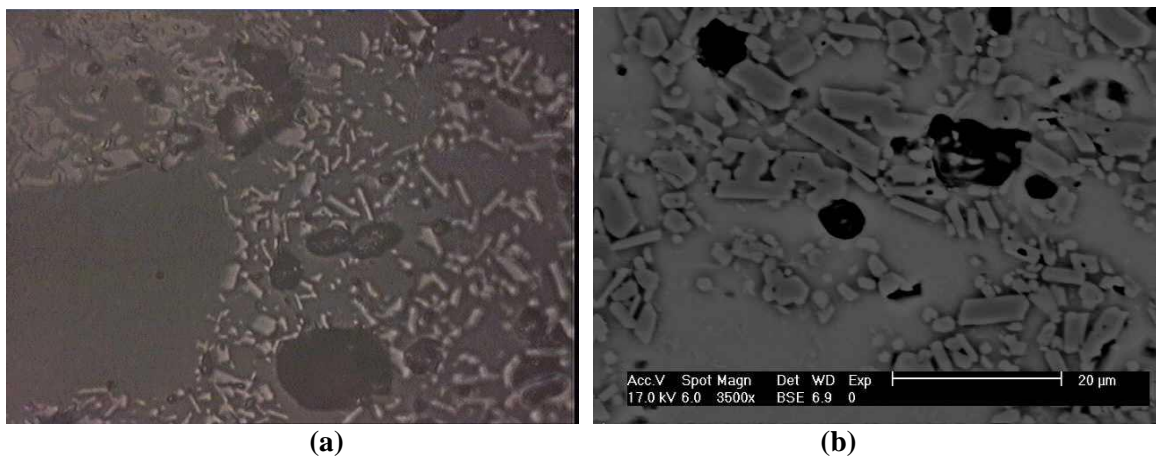**Figure 9.** The XRD pattern of the unused refractory brick (GS-M-Unused)

(a)   (b)

Figure 10. (a) RL optical microscope image of the unused refractory brick (1500x). **(b)** SEM image of the unused refractory brick
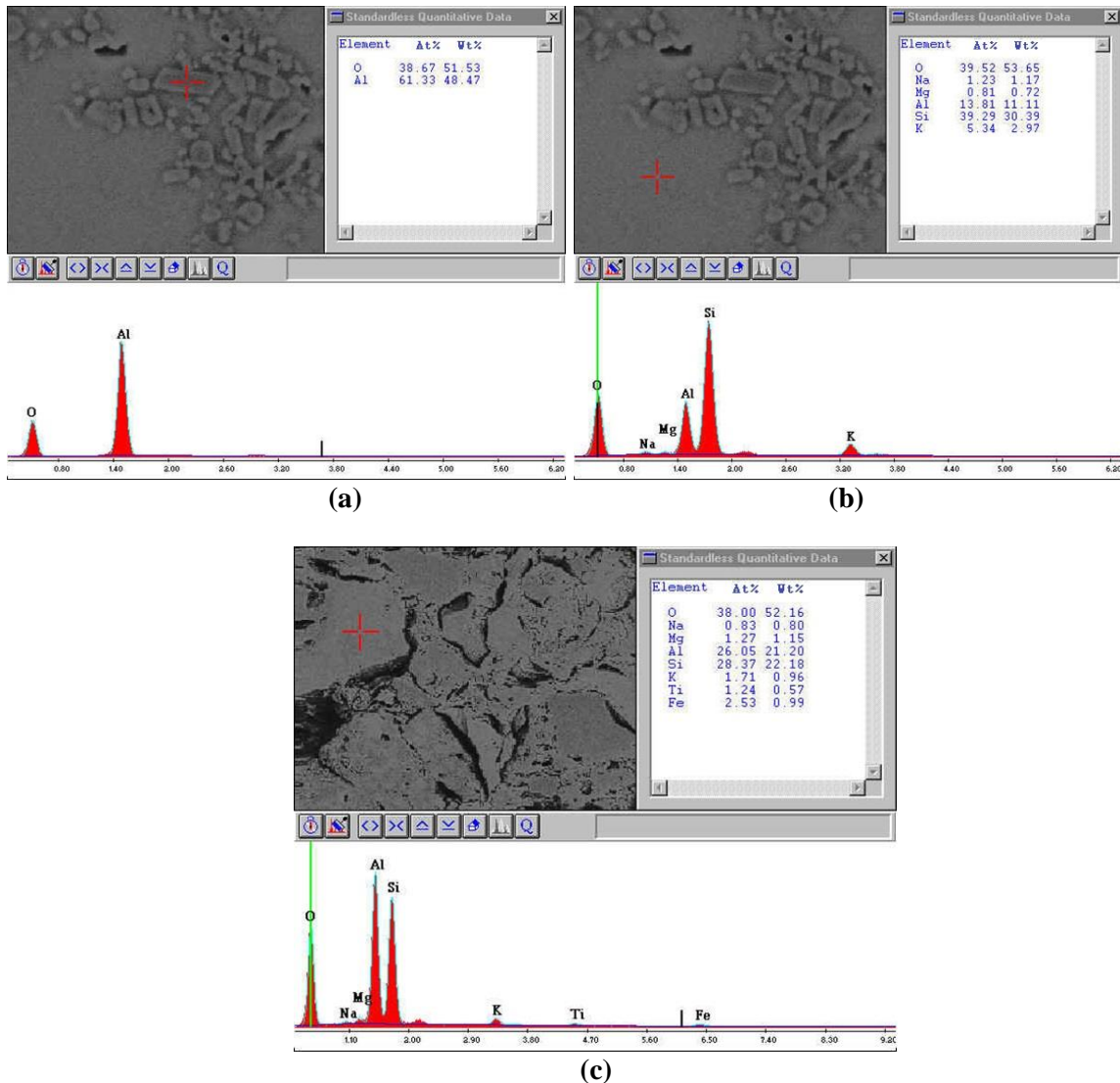
Figure 11. (a) EDS analysis of crystals of size ~ 7 μm embedded in the matrix of the unused refractory brick **(b)** EDS analysis of the glass matrix of the same unused refractory brick, **(c)** EDS analysis of a large grain in the structure

G-Mor Samples:

The XRD pattern of the mortar layer (Figure 12) showed that the crystalline phase was almost entirely mullite. The mortar layer was easily discernable by unaided eye as a dark gray region. The RL-OM image of the mortar layer is given in Figure 13. The crystal structure and the glassy matrix did not show any discernable differences for the regions near and far from the corrosion interface. There was not any detectable freeze plane also for the mortar. These observations further pointed out that the corrosion mechanism was direct dissolution of the refractory material in the molten glass. The mullite crystal sizes were ~14 μm on the average. The porosity of the corroded mortar layer was approximately 40% with pore sizes up to 1mm.
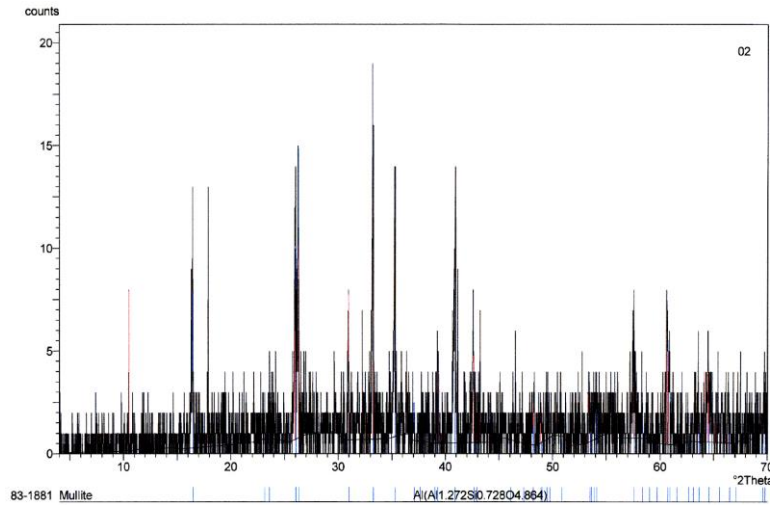
Figure 12. The XRD pattern of the corroded mortar connecting refractory bricks

Figure 13. RL-OM image of the corroded mortar connecting the refractory bricks

GB-AZS Samples:

The XRD pattern of the corroded electrofused cast AZS block showed that the only crystal forms comprising the refractory were ZrO_2 and corundum (Figure 14). This might point out to the possibility that the amount of mullite crystals was too low to be detected by the XRD.

The microstructural analysis of the corroded electrofused cast AZS brick (GB-AZS) was carried out by RL-OM and SEM-EDS analyses. The related images are shown in Figure 15a and 15b. Although the grain structure of the molten glass interface was different from the relatively unaffected bulk, it was not possible to detect any freeze plane. The examination of the interface did not show any solid product accumulation, evidencing the direct dissolution mechanism.

The EDS analyses of various features in the structure are shown in Figure16. The refractory block contained ZrO_2 crystals widespread throughout the body. Large corundum grains existed in little quantities. The matrix contained mullite crystals embedded in a glass phase of Si, Al, K, and Na. The service life of AZS refractory pavers was observed to be longer in comparison to the GS-M refractory bricks.
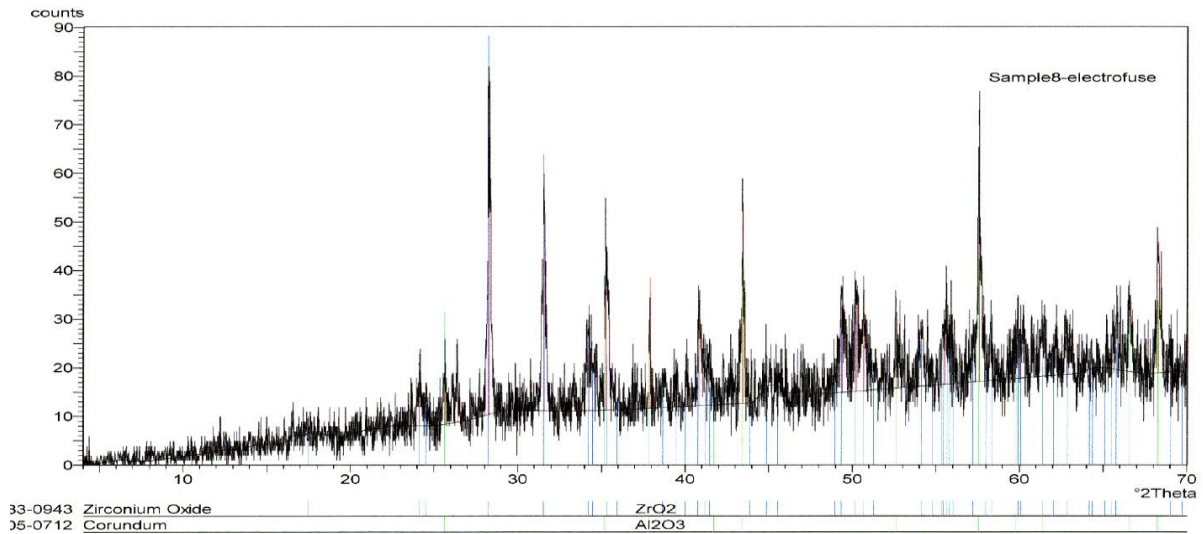
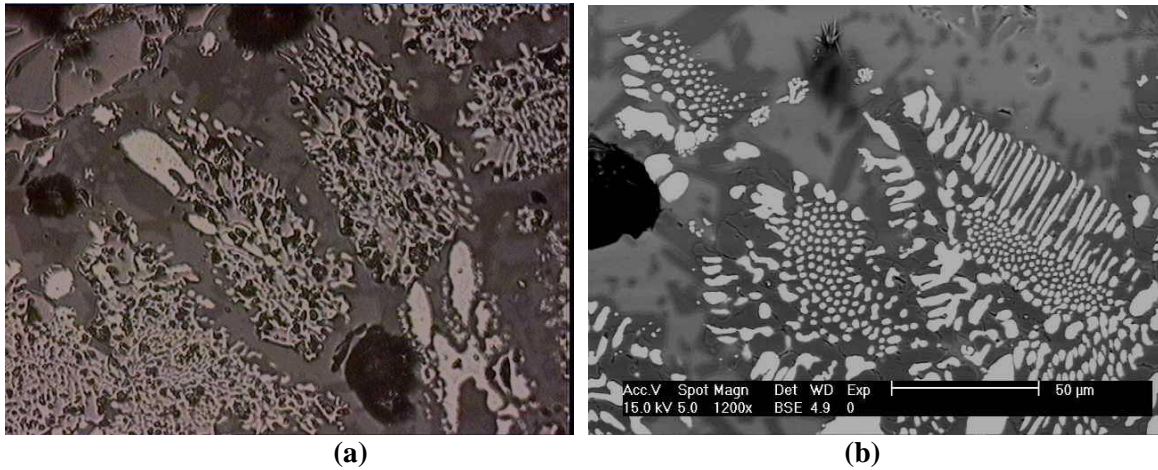**Figure 14.** XRD pattern of the corroded electrofused cast AZS refractory

(a)	**(b)**

Figure 15. (a) RL-OM image of the electrofused cast AZS refractory, inner bulk, **(b)** SEM image of the same refractory, inner bulk

Frit Compositions:

The compositions of the molten glasses (frit) produced in the industrial furnace are given in Table 2. The molten glass coded as transparent-1 was shown to be almost entirely amorphous by the XRD analysis, and it had the relative proportions of 9.0 % K_2O, 13.6% Al_2O_3, and 77.4% SiO_2. This point was marked as circled cross in the ternary phase diagram in Figure 17.

The Relevant Ternary Phase Diagram:

In the examined GS-M refractory the most abundant compounds were that of Al_2O_3, SiO_2, and K_2O. Therefore, by predicting the effect of the molten glass on these compounds by the use of the ternary phase diagram of K_2O-Al_2O_3-SiO_2 given in Figure 17, it would be possible to predict the corrosion behavior of the refractory in the molten glass environment.
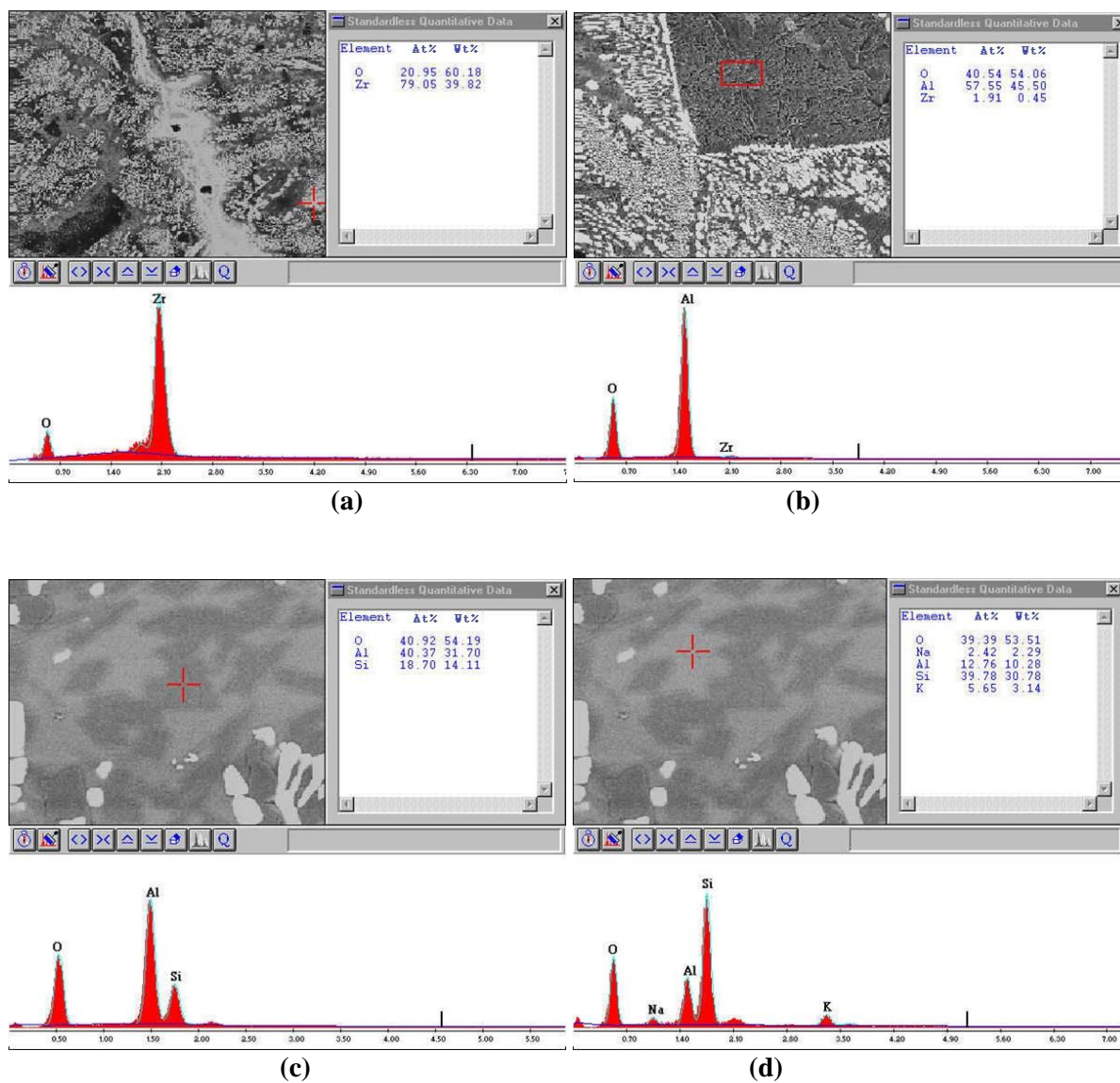
Figure 16. **(a)** EDS analysis of widespread ZrO_2 crystal grains **(b)** EDS analysis of corundum grain **(c)** EDS analysis of mullite crystals **(d)** EDS analysis of glassy matrix

Table 2. Empirical formulas of the frits

Transparent-1:

$$\left.\begin{array}{l}1.35B_2O_3\\0.72K_2O\\0.00Na_2O\\1.73ZnO\\0.00BaO\\1.65CaO\\0.59MgO\end{array}\right\}1.00Al_2O_3\left\{\begin{array}{l}9.65SiO_2\\0.00ZrO_2\end{array}\right.$$

Transparent-2:

$$\left.\begin{array}{l}1.12B_2O_3\\0.68K_2O\\0.00Na_2O\\1.39ZnO\\0.00BaO\\1.56CaO\\0.56MgO\end{array}\right\}1.00Al_2O_3\left\{\begin{array}{l}9.60SiO_2\\0.00ZrO_2\end{array}\right.$$

Opaque-1:

$$\left.\begin{array}{l}2.08B_2O_3\\1.23K_2O\\0.00Na_2O\\2.40ZnO\\0.25BaO\\3.33CaO\\0.79MgO\end{array}\right\}1.00Al_2O_3\left\{\begin{array}{l}19.09SiO_2\\1.35ZrO_2\end{array}\right.$$

Opaque-2:

$$\left.\begin{array}{l}2.72B_2O_3\\1.29K_2O\\0.00Na_2O\\3.24ZnO\\0.30BaO\\5.41CaO\\0.00MgO\end{array}\right\}1.00Al_2O_3\left\{\begin{array}{l}20.91SiO_2\\1.76ZrO_2\end{array}\right.$$

Opaque-3:

$$\left.\begin{array}{l}2.82B_2O_3\\1.28K_2O\\0.00Na_2O\\1.09ZnO\\0.00BaO\\3.18CaO\\2.37MgO\end{array}\right\}1.00Al_2O_3\left\{\begin{array}{l}14.93SiO_2\\0.97ZrO_2\end{array}\right.$$

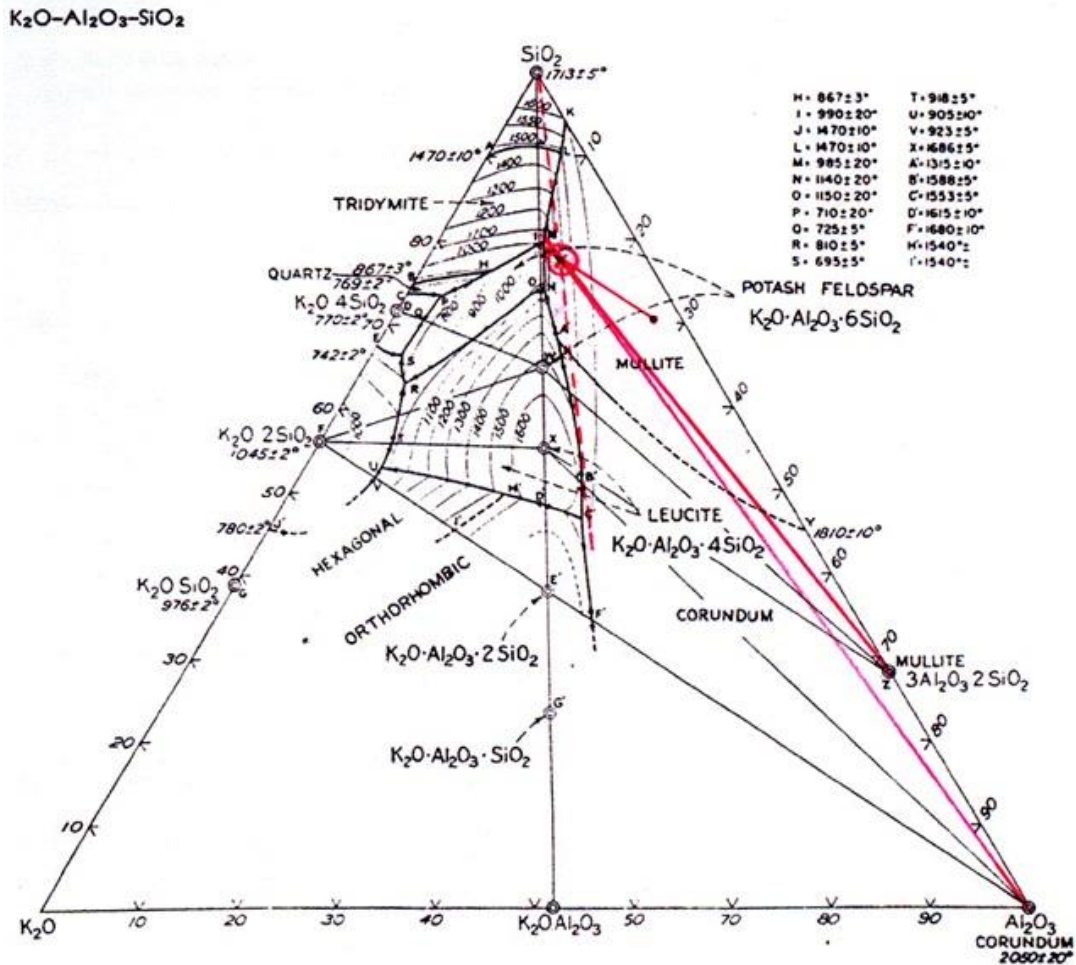**Figure 17.** System K_2O-Al_2O_3-SiO_2 [21]

The liquidus temperature for the transparent-1 molten glass composition which is in the primary crystallization field of mullite is 1340°C. Between 1040°C to 1340°C mullite will be fused from the refractory. Between the eutectic at 1000°C to 1040°C mullite and tridymite (SiO_2) will be fused together. At 1000°C potash feldspar ($K_2O.Al_2O_3.6SiO_2$), tridymite, and mullite fuses to the molten glass. Corundum in contact with the given molten glass will fuse at 1050°C. Only SiO_2 can survive before fusing slightly over 1600ºC. The glassy phase of the refractory, the EDS analysis of which is given in Figure 8b, had the relative composition of 3.1 % K_2O, 26.3% Al_2O_3, and 70.6% SiO_2. Alarmingly, this composition is in equilibrium with the molten glass at slightly lower than 1000°C.

Given the operating temperature as 1470±20°C the glassy phase, mullite crystals, corundum grains will fuse into the molten glass. Since the concentration of SiO_2 in the molten glass is higher as compared to Al_2O_3 and K_2O, the driving force for the dissolution of both Al_2O_3 and K_2O (depending on their saturation solubilities at 1470°C) is higher as compared to SiO_2. Chemical corrosion by direct dissolution into the molten glass is the dominant mechanism of wear. The rate of wear is increased by the first push exudation, causing erosion in the form of mechanical spalling.

Potential Effects of Other Constituents:

Considering that B_2O_3 exists as 8.5% in the frit composition the fusion temperatures are expected to be lower than the above values. However, the other existing compounds, CaO, MgO, ZnO will tend to increase the fusion temperatures [21]. The ZrO_2 contained in the refractory brick, though in low proportions, extends the service life of the brick. As indicated by the liquidus curves, the lowest fusion temperature of Fe_2O_3-ZrO_2 system is 1500°C, TiO_2- ZrO_2 system is 1610°C, SiO_2- ZrO_2 system is 1660°C, and Al_2O_3- ZrO_2 system is 1900°C, which are all above the operating temperature [21].

The opaque frit which was shown to be almost entirely amorphous by XRD, contained 7.8% ZrO_2, making the liquidus temperatures over the operating temperature for almost all of the species comprising the refractory. In this case the dominant wear mechanism could be the mechanical spalling effect of the first push exudation. The in-situ service life of the same refractories in the furnace producing opaque frit was known to be much longer. The furnace producing transparent frits would require the complete renewal of its refractory lining in a period of 16 months while the furnace producing opaque frits had shown no sign of wear during the same service period.

4. CONCLUSIONS

The microstructure of corroded refractory brick, forming the sides of the molten glass tank of the frit furnace, was examined. The refractory was shown to comprise of corundum grains (with sizes up to 2 mm), large idiomorphic mullite grains (with sizes up to 2 mm), embedded in a porous matrix of mullite crystals (approximately 7 µm), and a glassy phase of the oxides of Si, Ca, Mg, K, Na.

Although the microstructure did not show much difference between the refractory-molten glass interface and the inner bulk, the Al_2O_3 content of the corrosion interface was higher compared to the inner bulk and unused brick. The porosity and the size of the pores in the corroded refractory were higher as compared to the unused refractory brick of the same type. The large pores of sizes up to 1 mm encountered in the corroded brick and the mortar constituted evidence to the exudation phenomenon.

The phase diagram analysis for the dissolution of the refractory brick in the molten glass of known composition (transparent 1) showed that the glassy matrix in the refractory would start to fuse at temperatures slightly lower than 1000°C. The results conformed to the fact that the saturation concentrations of these species were higher than their concentrations in the molten glass. A very

corrosive condition prevailed for the refractory in use, since the operating temperature was $1470°C$. Chemical corrosion by direct dissolution into the molten glass was the dominant mechanism of wear.

The same refractory bricks in contact with the molten glass containing 7.8 wt% ZrO_2 showed no sign of wear during the same service period. The AZS bottom pavers' service life was also longer compared to the mullite bricks. The lowest fusion temperature for most of the R_xO_y-ZrO_2 systems was $1500°C$ which was above the operating temperature, and the major mechanism for erosion was the mechanical spalling effect of the first push exudation.

This study forms the basis of further studies for the optimization of the operating capacities of such furnaces maximizing the time cumulative frit output, that is, a compromise between the increased molten glass flow rate that will increase the erosion rates of the furnace refractories, and the increased production capacity.

ACKNOWLEDGEMENT

REFERENCES

[1] Singer F, Singer SS. Industrial Ceramics. London, GB: Chapman and Hall Ltd., 1963.

[2] Bull AC. Bodies, Glazes, and Colours for Fast Firing. British Ceramic Transactions 1982; 81: 69-74.

[3] Hare TM. Ceramics (Thermal Treaatment). In: Howe-Grant M, editor. Kirk-Othmer Encyclopedia of Chemical Technology. 4th ed. Vol. 5. New York, USA: John Wiley and Sons, 1991, pp.260-266

[4] Burzacchini B, Paganelli M, Christ GH. Examination of Fast-Fire Frits and Glazes Using a Hot Stage Microscope at Different Heating Rates. Ceramic Engineering and Science Proceedings 1996; 17(1): 60-66.

[5] Karasu B, Dolekcekic E, Ozdemir B. Compositional modifications to floor tile glazes opacified with zircon. British Ceramic Transactions 2001; 100(2): 81-85.

[6] O'Conor E, Eppler RA. Semicrystalline Glazes for Low Expansion Whiteware Bodies. Ceramic Bulletin 1973; 52(2) 180-184.

[7] Manfredini T, Pellacani GC. Tile Whiteware. In: Schneider SJ, editor. Engineered Materials Handbook, Vol. 4. New York, USA: ASM, 1991, pp.925–929.

[8] Brusa A, Bresciani A. Floor and Wall Tile Production Through a Multipurpose Body. Ceramic Engineering and Science Proceedings 1996; 17(1): 50-59.

[9] Casasola R, Rinco´n JM, Romero M. Glass–ceramic glazes for ceramic tiles: a review. Journal of Materials Science 2012; 47(2): 553-582.

[10] Akkurt S. Prediction of the slag corrosion of MgO-C ladle refractories by the use of artificial neural networks. Euro Ceramics VIII, Part 1-3. Key Engineering Materials 2004; 264-268: 1727-1730.

[11] Akkurt S, Leigh HD. Corrosion of MgO-C ladle refractories. American Ceramic Society Bulletin 2003; 82(5): 32-40B.

[12] Balikoglu F, Akkurt S. Isothermal corrosion testing of frit furnace refractories. Ceramics International 2009; 35: 3411-3419.

[13] Kingery WD, Bowen HK, Uhlmann DR. Introduction to Ceramics. 2nd ed. New York, USA: John Wiley and Sons, 1976.

[14] McCauley RA. Corrosion: A Review of Some Fundamentals. In: Pecoraro, GA, Marra J, Wenzel JT, editors. Corrosion of Materials by Molten Glass. Westerville, Ohio, USA: The American Ceramic Society, 1993. pp.81-89.

[15] Duvierre G, Copet B, Nelson MA. Use of Fused-CastAZS Products and Their Monolithic Derivatives in Applications for the Ceramic Industry. In: Pecoraro, GA, Marra J, Wenzel JT, editors. Corrosion of Materials by Molten Glass. Westerville, Ohio, USA: The American Ceramic Society, 1993. pp.105-129.

[16] Zhang S, Lee WE. Use of Phase Diagrams in Studies of Refractories Corrosion. International Materials Reviews 2000; 45(2): 41-58.

[17] Petreanu JP, Colangelo SE, Brown DL. Corrosion of Dense Chromic Oxide Refractory in E Glass. In: Pecoraro GA, Marra J, Wenzel JT, editors. Corrosion of Materials by Molten Glass. Westerville, Ohio, USA: The American Ceramic Society, 1993. pp.171-178.

[18] Winder SM, Selkregg KR. Exudation and Corrosion Behavior of Fusion Cast AZS Refractories. In: Pecoraro GA, Marra J, Wenzel JT, editors. Corrosion of Materials by Molten Glass. Westerville, Ohio, USA: The American Ceramic Society, 1993. pp.131-153.

[19] Karakus M, Moore RE. Post-Mortem Study of Glass Melting Furnace Refractories. In: Pecoraro GA, Marra J, Wenzel JT, editors. Corrosion of Materials by Molten Glass. Westerville, Ohio, USA: The American Ceramic Society, 1993. pp.179-181.

[20] Asakura H, Ikegami K, Mamoru M, Wakita H. Determination of Components in Refractories Containing Zirconia by X-Ray Fluorescence Spectrometry. X-Ray Spectrometry 2000; 29[6]: 418-425

[21] Levin EM, McMurdie HF, Hall FP. Phase Diagams for Ceramists. Westerville, Ohio, USA: American Ceramic Society, 1956.